IOPscience iopscience.iop.org

Home Search Collections Journals About Contact us My IOPscience

Oxygen Induced Phase Changes in $YBa_2Cu_3O_{6+\delta}$. Transport, Structural and Spectroscopic Evidence

This article has been downloaded from IOPscience. Please scroll down to see the full text article.

1989 Phys. Scr. 1989 82

(http://iopscience.iop.org/1402-4896/1989/T25/013)

View the table of contents for this issue, or go to the journal homepage for more

Download details:
IP Address: 130.199.3.165
The article was downloaded on 23/08/2012 at 13:47

Please note that terms and conditions apply.

Physica Scripta. Vol. T25, 82–87, 1989.

Oxygen Induced Phase Changes in $YBa_2Cu_3O_{6+\delta}$. Transport, Structural and Spectroscopic Evidence

H. Kuzmany, M. Matus and E. Faulques*

Institut für Festkörperphysik, University of Vienna, and Ludwig Boltzmann Institute für Festkörperphysik, Strudlhofgasse 4, A-1090 Vienna, Austria

and

S. Pekker, Gy. Hutiray, É. Zsoldos and L. Mihály

Central Research Institute for Physics, POB 49, Budapest 1525, Hungary

Received April 6, 1988; accepted June 22, 1988

Abstract

$YBa_2Cu_3O_{6+\delta}$ was prepared for various values of δ by equilibrating pieces of fully oxidized orthorhombic and fully reduced tetragonal material at 600°C. T_c was found to decrease rapidly with decreasing δ and reached zero completely within the orthorhombic phase. Strong changes in frequency and intensity of Raman and IR spectra were observed and could be correlated to the structural changes. In particular two IR-active modes at 580 cm^{-1} and at 630 cm^{-1} were observed which allowed to observe directly the doping process by the O(1)-oxygen. Also, the ratio of two special Raman lines was found to be a critical function of the oxygen concentration. From the experiments an assignment of vibrational modes was obtained in very good agreement with a recent normal coordinate calculation.

1. Introduction

Since the discovery of superconductivity in the ceramic perovskites [1, 2] the oxygen treatment of the samples was found to play a crucial role for the structural and transport properties of the materials. This holds in particular true for the family of YBaCuO where a very strong dependence of the transition temperature to superconductivity (T_c) and of the superconducting volume fraction on the oxygen concentration in the samples has been reported [3–10]. In addition a transition from a tetragonal D_{4h}^1–P4/mmm phase for low oxygen concentration to an orthorhombic D_{2h}^1–Pmmm phase for high oxygen concentration was reported in these materials. This structural change occurs between an oxygen stoichiometry of $O_{6.3}$ and $O_{6.5}$ depending on the technique used for establishing a specific oxygen concentration. This is either done by quenching the samples from high temperatures where the oxygen concentration is reduced to below $O_{6.1}$ or by equilibrating them in an atmosphere with reduced oxygen pressure or in a sealed tube with a well defined amount of oxygen getter.

We have recently reported preliminary results of a systematic study on transport and vibrational spectra of oxygen doped $YBa_2Cu_3O_{6+\delta}$ and $YBa_2Cu_{3-x}Zn_xO_{6+\delta}$ [11, 12]. In these experiments a special technique for oxygen doping was used which allowed to approach a well defined state of doping from the completely undoped ($\delta = 0$) as well as from the completely doped ($\delta = 1$) state of the samples [10]. In this paper we present an extended analysis of the experimental results. Particular attention is paid to the correlation between structural data on one side and transport properties, line positions and line intensities of vibrational Raman and IR spectra on the other side. Superconductivity disappeared within the orthorhombic phase and did not coincide with the orthorhombic to tetragonal transition. The change of the vibrational spectra with oxygen concentration gave additional information for the assignment of the vibrational modes. In particular clear evidence for the modes which involve the doping oxygen atom was obtained.

2. Sample preparation and experimental procedure

Sample preparation was performed from a standardized batch of nominally single phase $YBa_2Cu_3O_{6+\delta}$ as described previously [11]. The starting material was reground, repelleted and reheated for one day in air and subsequently equilibrated at 600°C in flowing oxygen. The previous assumption of $\delta = 1$ after this procedure was checked by Rietvelt analysis of neutron diffraction data and revealed a slightly smaller value of 0.9 for δ. Thus, all oxygen concentrations used in Refs. [11] and [12] had to be recalibrated. After the first oxidation process half of the total amount of the oxidized material was reheated in vacuum at 850°C and then cooled within two hours to room temperature in order to obtain the oxygen deficient reduced form of the ceramic. From the weight loss an oxygen concentration of 6.13 was found. The samples of $YBa_2Cu_3O_{6+\delta}$ with various δ were prepared by sealing well defined quantities of oxidized and reduced ceramics in quartz tube, equilibrating the system for 5 h at 600°C and additionally for 12 h at 500°C. Then the system was cooled in 20 h to room temperature. Figure 1 shows the change of the masses of the two pieces as normalized to 1 mg total mass and the difference between the loss of mass of the one piece and the gain of mass of the other piece. The very small value for the mass defect is a good proof for the proper equilibration of the two starting materials.

IR-spectra were obtained from compressed pellets with normalized quantities of ceramic material using both an FTIR spectrometer and a grating spectrometer. A weak line at 858 cm^{-1} was found in all IR spectra and identified to originate from a very small (0.5%) contamination of a carbonate. This carbonate is assumed to be a small rest of unreacted starting material accumulated in grain boundaries. The absorption of this line was used as an internal standard for intensity calibration which is of crucial importance in the

* Permanent address: Institut de Physique et Chimie des Materiaux, Universite de Nantes, F-44072 Nantes, France.

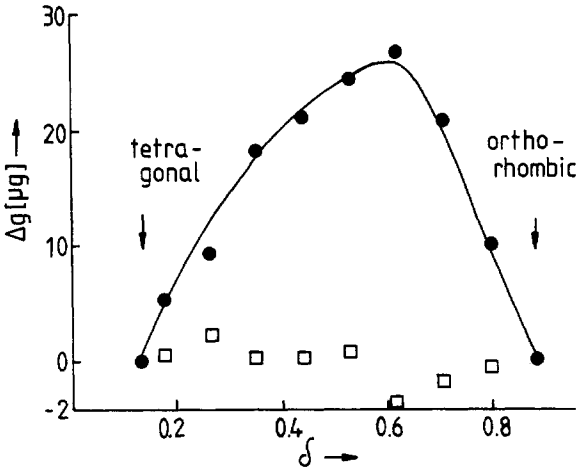

Fig. 1. Change of masses during equilibration of oxidized and reduced YBaCuO for various compositions (full points) and difference between the gain of mass of the reduced and loss of mass for the oxidized sample (squares).

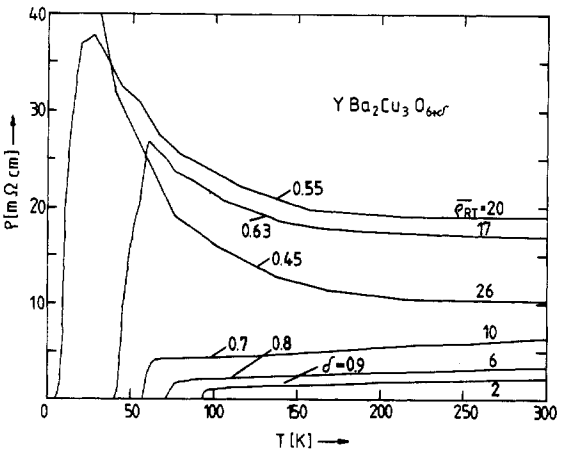

Fig. 3. Specific resistivity versus temperature for various oxygen concentrations; ϱ_{RT} is the room temperature resistivity averaged over several sample from the same batch.

present experiments since the conductivity and simultaneously the penetration depth of the IR-radiation changes by several orders of magnitude with doping. Raman spectra were obtained with a 200 mW line focus laser excitation at 488.0 nm and photon counting detection. IR and Raman experiments were performed at room temperature.

The conductivity was measured between 4.2 K and room temperature by an ac and dc 4 point technique. The unit cell parameters were determined by fitting 20–25 well defined and indexed X-ray diffraction pattern. No systematic difference between the pieces of the material which were originally fully oxidized and those which were originally fully reduced occured, though in some experiments and particular in those concerning the transport properties strong scattering of experimental results was observed.

3. Experimental results

Figure 2 shows the lattice constants for the originally fully oxidized (full points) and for the originally fully reduced samples (squares) as a function of the oxygen concentration δ. Within experimental error there is no difference between the two types of materials. The room temperature structure changes from orthorhombic to tetragonal between $\delta = 0.36$ and 0.45. The very high room temperature resistivity of the oxygen deficient sample ($\delta = 0.13$) drops by several orders of magnitude until the concentration for the orthorhombic to tetragonal transition ($\delta \approx 0.4$) is reached. From here only a weak further decrease of the resistivity occured for doping concentrations up to $\delta = 0.9$. Thus, the room temperature resistivity correlates with the room temperature structure.

Figure 3 shows the temperature dependence of the resistivity for samples with various doping concentration. For oxygen stoichiometry of 6.45 no superconductivity is obtained but the room temperature resistivity is still in the metallic range. Figure 4 shows that in contrast to the behaviour of the room temperature resistivity the low temperature resistivity does not scale with the difference between the unit cell parameters a and b as a function of the oxygen concentration. Superconductivity is definitely quenched in the shaded area between $\delta = 0.45$ and 0.54 where both the originally orthorhombic and the originally tetragonal sample are in the orthorhombic phase. Superconductivity in samples with $\delta = 0.45$ was not observed for temperatures as low as 1 K.

Infrared absorption from vibrational modes for various values of δ were observed. The background of free carrier

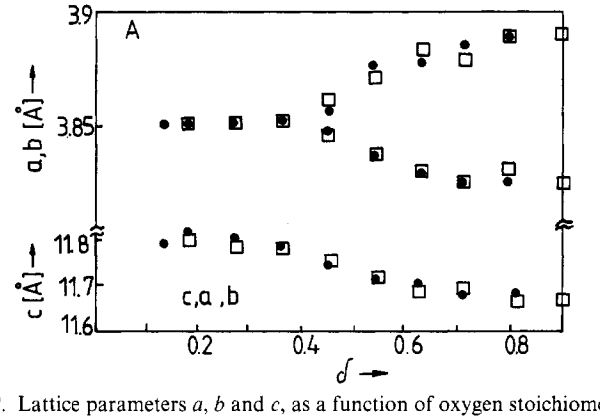

Fig. 2. Lattice parameters a, b and c, as a function of oxygen stoichiometry δ; (○) for originally orthorhombic samples, (□) for originally tetragonal samples.

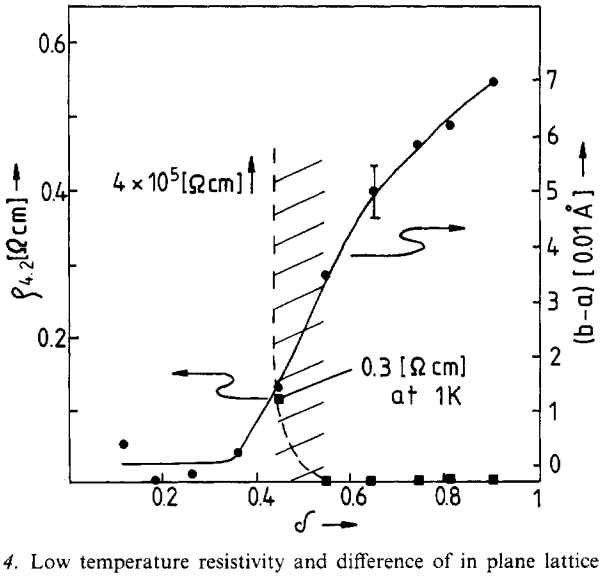

Fig. 4. Low temperature resistivity and difference of in plane lattice parameters versus oxygen stoichiometry δ.

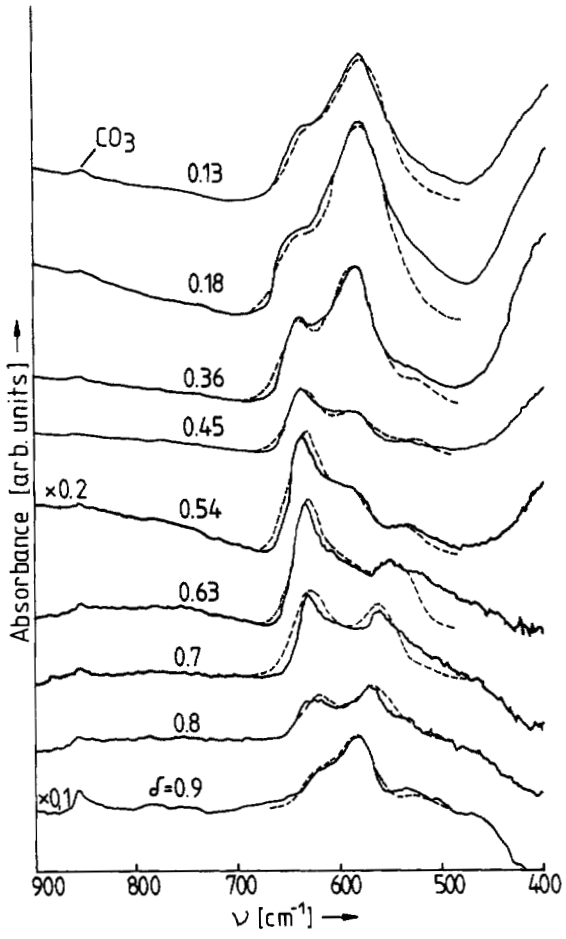

Fig. 5. IR absorbance for $YBa_2Cu_3O_{6+\delta}$ for various states of oxygen stoichiometry. The dashed lines are oscillator fits with a Gaussian line shape.

absorption strongly increased and contrary the vibrational absorption intensity continuously decreased with oxygen doping. Figure 5 presents spectra for δ between 0.9 and 0.13. The most prominent change is the continuous decrease of the peak at 585 cm^{-1} with increasing oxygen concentration and the simultaneous increase and shift of a mode starting at about 515 cm^{-1} in the weakly doped region and ending at 580 cm^{-1} in the heavily doped material. Since the bands from

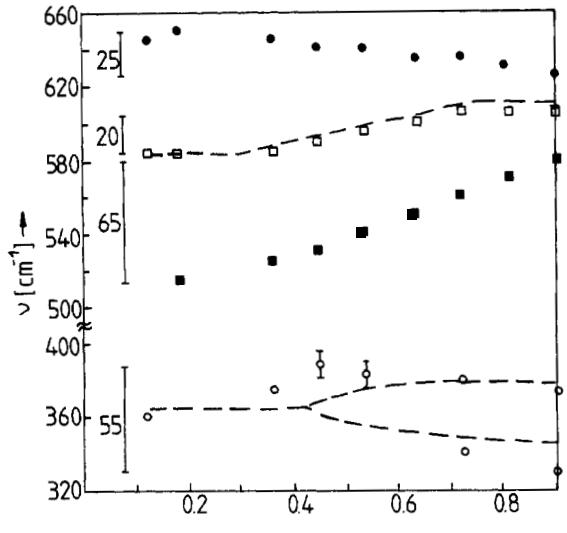

Fig. 6. Frequency shift of IR modes between 320 cm^{-1} and 640 cm^{-1} versus δ. The dashed lines are plots for $c^{-3.3}$, a^{-4} and b^{-4}.

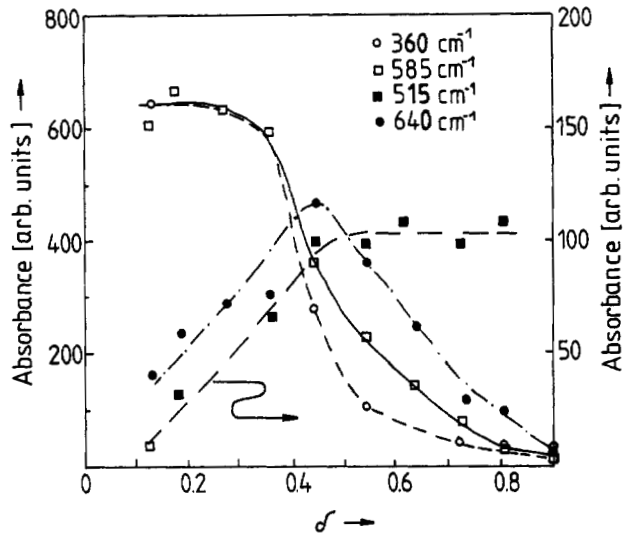

Fig. 7. Infrared absorbance for various lattice modes versus δ.

the individual modes overlap strongly and the change of penetration depth of the IR radiation simulates a decreasing vibrational absorption a further interpretation of the results is only possible if the individual spectra are calibrated with respect to absorption intensity by the small line assigned as CO_3 in the Figure and by fitting the structures in the spectra with individual oscillators. The dashed lines are trial and error results for a fit with Gaussian lineshapes for the individual modes.

Figure 6 yields the line position for various modes as a function of oxygen concentration. Line shifts can be as large as 65 cm^{-1}. The line at 360 cm^{-1} splits for high oxygen concentrations. The large error bars at intermediate values of δ mean that the mode is already split but the two lines are not yet resolved. This behaviour and also the line shift of the

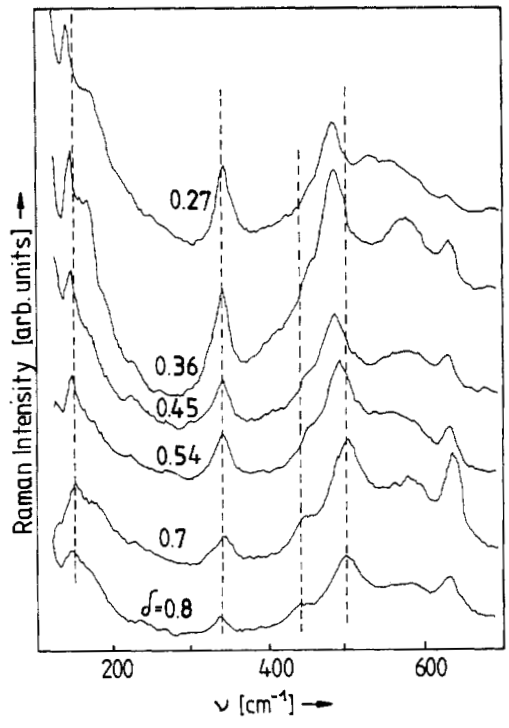

Fig. 8. Raman spectra of $YBa_2Cu_3O_{6+\delta}$ as excited with a blue laser at 488.0 nm for various values of δ.

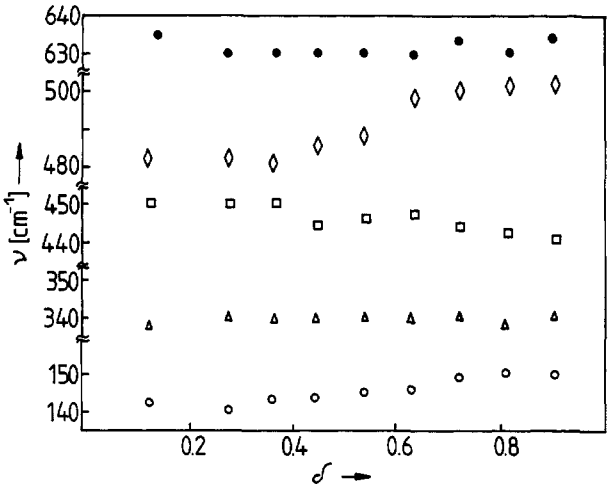

Fig. 9. Frequency shift of Raman modes between 140 cm^{-1} and 640 cm^{-1} versus δ.

mode around 580 cm^{-1} appears to be strongly related to the change of te unit cell parameters with doping. The frequency of the mode typically scales with some high power of the lattice parameters. The dashed lines in the figure indicate $c^{-3.3}$ and a^{-4} or b^{-4} for the modes at 580 cm^{-1} and at 360 cm^{-1}, respectively. For the other lines no direct relation to the unit cell parameters is observed. The change of the absorption intensities for the individual lines is even more dramatic as shown in Fig. 7. The modes at 360 cm^{-1} and at 585 cm^{-1} exhibit a strong decrease in absorption with doping even after the calibration with the carbonate line. On the contrary, the mode starting at 515 cm^{-1} and the mode at 640 cm^{-1} increase first and then after the orthorhombic phase is reached saturate or even decrease with further doping. This behaviour discriminates the individual modes with respect to their origin and with respect to their interaction with the carriers induced by the doping process.

Raman spectra of the ceramics are compiled in Fig. 8 for various values of δ. The changes with doping are not as dramatic as for the IR-spectra but a line shift for the mode at 502 cm^{-1} and an increase of scattering intensity for the mode at 340 cm^{-1} is well established. Intrinsic lines were found at 150 cm^{-1}, 340 cm^{-1}, 440 cm^{-1}, and 502 cm^{-1} in the oxidized sample. Several of the Raman peaks are spurious and not observed in all samples. Particularly the line at 630 cm^{-1} varied strongly from sample to sample and the use of a line focus for the laser is essential to obtain reproducible scattering intensities even within one sample.

Figure 9 presents the shifts of the Raman lines with doping. The shift of the 502 cm^{-1} line turns out to be non-linear with the doping concentration and again scales with the behaviour of the z-axis unit cell parameter. Intensities of Raman lines are usually more difficult to analyse as compared to absorptions of IR-lines because scattering intensities depend strongly on sample surface condition and sample alignment. Accordingly, a strong scattering is seen in the plot of Raman intensities versus oxygen concentration as shown in Fig. 10A for the mode at 150 cm^{-1}. Nevertheless a linear trend for the change of line intensities with δ can be estimated from the graph. Assuming linear behavior for this line, we can obtain scaling factors for the rest of the lines in the spectrum. Indeed, part B of the figure yields a very diversified but smooth change of scattering intensities with δ for the other intrinsic lines. Of particular interest is the behaviour of the Raman peak at 630 cm^{-1} which starts near zero for low doping concentrations, reaches a peak value near $\delta = 0.7$ and decays again for larger values of δ. An even smoother behaviour of Raman intensities versus oxygen concentration is obtained for the peak intensity ratio of the line at 340 cm^{-1} and 502 cm^{-1} as shown in Fig. 11. This ratio may thus be used to determine oxygen concentrations in thin films or single crystals where the technique of determining the weight change or neutron diffraction can not be applied because of the low involved sample masses.

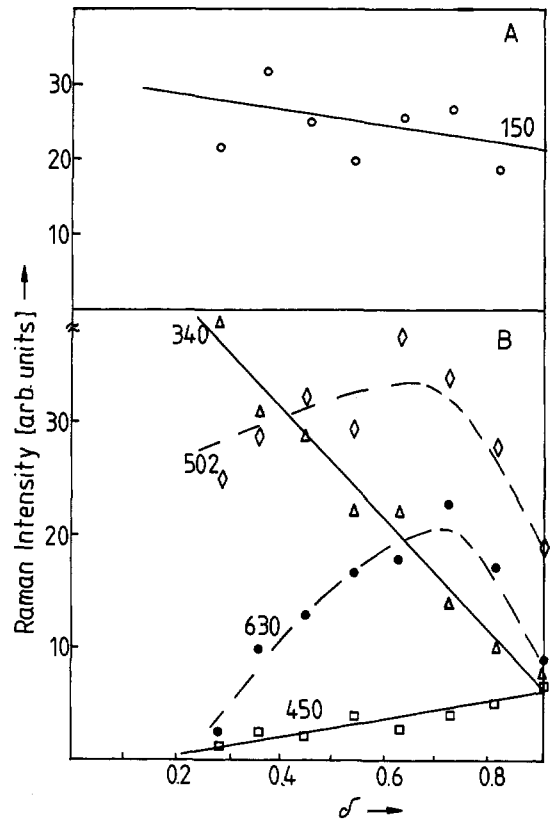

Fig. 10. Raman line intensities versus oxygen concentration. A shows the row data for the line at 150 cm^{-1}. In B the intensities are rescaled according to the assumption that the 150 cm^{-1} line follows a linear δ dependance.

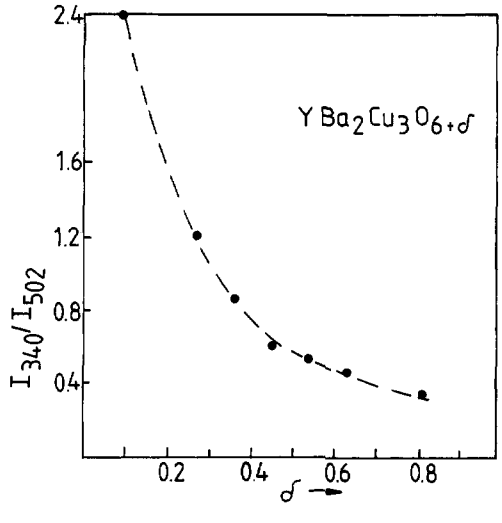

Fig. 11. Intensity ratio of Raman lines at 340 cm^{-1} and 502 cm^{-1} versus δ.

4. Discussion

The agreement of the lattice parameters for the material oxidized from the tetragonal phase and reduced from the orthorhombic phase indicates that for each doping concentration an equilibrium state is reached. The tetragonal to orthorhombic transition at room temperature occurs in both cases between $\delta = 0.36$ and 0.45 which is below the critical stoichiometry for which Cu is nominally 2+ and the oxygen $2p$ bands are expected to be full [13]. For the $\delta = 0.45$ sample the room temperature conductivity is high with a still nonmetallic temperature dependence. Fluctuations of the doping concentration on the one hand and disorder induced localization on the other hand may be the reason for these results. The final loss of superconductivity is decoupled from this behaviour and occurs well within the orthorhombic structure. Samples with an oxygen stoichiometry of 6.45 seem to be most interesting, since they exhibit a very high room temperature conductivity, a nonmetallic temperature dependence of the conductivity but no transition to superconductivity down to 1 K.

For an analysis of the vibrational spectra an assignment of atomic positions as O(1), O(4), and O(2, 3) for the oxygens along the b and c direction and in the corrugated a, b plane, respectively, is convenient. Similarly, the copper atoms in the chains along b and in the planes are Cu(1) and Cu(2), respectively. Tentative assignments of various Raman and IR active modes and preliminary discussions on the influence of oxygen deficiency on the vibrational spectra have been reported by several authors [14–21]. We may use the response of line position and line intensity on the oxygen doping as an additional tool to identify individual modes. The close correlation between the lattice parameter along the z-axis and the IR active mode at 585 cm^{-1} and the Raman active mode at 502 cm^{-1} suggests that these modes have a normal coordinate essentially parallel to z. On the other hand, the splitting of the line at 360 cm^{-1} for oxygen concentrations leading to the tetragonal to orthorhombic phase transition suggests that their normal coordinate is mainly in the a, b plane. The strong shift of vibrational frequency for the mode at 515 cm^{-1} could be due to a change of Cu valency during the doping process in agreement with a recent XANES experiment on quenched samples [22].

The very diversified behaviour of the intensities of the IR active modes is a consequence of their different origin and different response to the electronic system. The modes at 360 cm^{-1} and at 585 cm^{-1} represent the generally expected decrease of dipole oscillator strength due to the shielding effect of free carriers. The increase of the absorption for the modes at 515 cm^{-1} and at 640 cm^{-1} is unusual and suggests that these modes involve essentially the doping atom 0(1). For doping concentrations in the range of the orthorhombic structure the free carrier shielding inhibits a further increase of the total oscillator strength. Apparently it has a different effect on the two modes which suggests that they have a different orientation to the two-dimensional charge carrying a, b plane. The mode at 640 cm^{-1} is oriented parallel to the plane and thus more strongly shielded by the carriers than the mode at 515 cm^{-1} which is oriented perpendicular to the a, b planes. This effect is very similar to the behaviour of the two Cu–O modes in $La_{2-x}Sr_xCuO_4$ which exhibit a very different response to the Sr doping [23, 24].

Table I. *The vibrational mode assignment of* $YBa_2Cu_3O_{6+\delta}$

(a) *Raman active modes*

Obs. [cm^{-1}]	Calc.	Assignment	Normal coordinate
150	159	A_g in D_{2h}	Cu(2) ∥ c
140	131	A_{1g} in D_{4h}	Cu(2) ∥ c
340	347	A_g in D_{2h}	O(2,3) ∥ c, asymm
	352	B_{1g} in D_{4h}	O(2,3) ∥ c, asymm
440	373	A_g in D_{2h}	O(2,3) ∥ c, symm
≈460	401	A_{1g} in D_{4h}	O(2,3) ∥ c, symm
502	515	A_g in D_{2h}	O(4) ∥ c
480	484	A_{1g} in D_{4h}	O(4) ∥ c

(b) *Infrared active modes*

Obs. [cm^{-1}]	Calc.	Assignment	Normal coordinate
328	361	B_{3u} in D_{2h}	O(4), O(1) ∥ a symm
377	429	B_{2u} in D_{2h}	O(4), O(1) ∥ b symm
360	355	E_u in D_{4h}	O(4) ∥ a, b symm
515–580	555	B_{1u} in D_{2h}	O(4), O(1) ∥ c asymm
585	540	A_{2u} in D_{4h}	Cu(1), O(4) ∥ c asymm
640	675	B_{2u} in D_{2h}	Cu(1), O(1) ∥ b asymm

An interesting result is obtained for the Raman intensities of the non intrinsic Raman active mode at 630 cm^{-1}. It had been suggested that it results from O(1)–Cu(1) motion [25] which in a perfect crystal is Raman forbidden. Defects may break the selection rules and render the line visible in the Raman spectrum. This explains why the intensity of the line is strongly sample dependent. The smooth increase and final decrease of the intensity of this line, shown in Fig. 10B, is indeed a straightforward consequence of this interpretation. The increase represents the increasing O(1) concentration while the decrease arises from the increasing order in the fully oxidized system. At some intermediate δ value the high 0(1) concentration and the high degree of disorder leads to a peak in the intensity of the Raman line.

A final and individual assignment of the modes could be performed using the results of a force field calculation by W. Kress [26, 27]. The modes for the orthorhombic phase are distributed at $5A_g + 5B_{2g} + 5B_{3g} + 7B_{1u} + 7B_{2u} + 7B_{3u}$ and at $4A_{1g} + B_{1g} + 5E_g + 5A_{2u} + B_{2u} + 6E_u$ for the tetragonal phase. Table 1 summarizes these assignments which take care for all details of the specific behaviour of the modes discussed above. The experimentally observed mode frequencies are in very good agreement with the results from the force field calculation also shown in the table.

5. Conclusion

In conclusion we demonstrated that $YBa_2Cu_3O_{6+\delta}$ is in an equilibrium state even at intermediate doping ranges and that the transition to superconductivity occurs within the orthorhombic phase. Vibrational spectra exhibit a strong response with respect to vibrational line position and with respect to line intensities to the oxygen doping. In particular it was possible to study the doping process by following the additional modes induced by the doping atom. The ratio of two special Raman line intensities was observed to represent a critical measure for the oxygen concentration in the ceramic.

Acknowledgements

This work was partly supported by the FFWF in Austria and by the OMFB in Hungary. One of the authors (EF) acknowledges the CNRS in France for granting a sabbatical leave. For the conductivity measurements down to 1 K and for the neutron diffraction analysis we acknowledge Dr. D. Schweitzer from the Max Planck Institute in Heidelberg and Dr J. Pannetier from the Laue-Langevin Institute in Grenoble, respectively.

References

1. Bednorz, J. G. and Müller, K. A., Z. Phys. **B64**, 189 (1986).
2. Chu, C. W., Hor, P. H., Meng, R. L., Gao, L., Huang, Z. J. and Wang, Y. Z., Phys. Rev. Lett. **58**, 405 (1987).
3. Oda, M., Murakami, T., Enomoto, Y. and Suzuki, M., Jpn. J. Appl. Phys. **26**, L804 (1987).
4. Kubo, Y., Yoshitake, T., Tabuchl, J., Nakabayashi, Y., Ochl, A., Utsumi, K., Igarashi, H. and Yonezawa, M., Jpn. J. Appl. Phys. **26**, L768 (1987).
5. Kishio, K., Shimoyama, J., Hasegawa, T., Kitazawa, K. and Fueki, K., Jpn. J. Appl. Phys. **26**, L1228 (1987).
6. Jorgensen, J. D., Veal, B. W., Kwok, W. K., Crabtree, G. W., Umezawa, A., Nowicki, L. J. and Paulikas, A. P., Phys. Rev. **B36**, 5731 (1987).
7. Ono, A., Jpn. J. Appl. Phys. **26**, L1223 (1987).
8. Oyanagi, H., Thara, H., Matsubara, T., Tokumoto, M., Matsushita, T., Hirabayashi, M., Murata, K., Terada, N., Yao, T., Iwasaki, H., Kumura, Y., Jpn. J. Appl. Phys. **26**, 1561 (1987).
9. Cava, R. J., Batlogg, B., Chen, C. H., Rietman, E. A., Zahurak, S. M. and Werder, D., Phys. Rev. **B36**, 5719 (1987).
10. Johnston, D. C. and Jacobson, A. J., Newsam, J. M., Lewandowski, J. T. and Goshorn, D. P., ACS Symposium Series Vol. 351 (Edited by D. L. Nelson, M. S. Wittingham and T. F. George), pp. 136–151, Am. Chem. Soc., Washington DC (1987).
11. Kuzmany, H., Matus, M., Faulques, E., Pekker, S., Hutiray, Gy., Zsoldos, É. and Mihaly, L., Solid State Commun. **65**, 1343 (1988).
12. Kuzmany, H., Faulques, E., Matus, M., Pekker, S., Zsoldos, É. and Mihály, L., Proc. Int. Conf. on High Temperature Superconductors, Interlaken (1988) (to be published).
13. Nücker, N., Fink, J., Fuggle, J. C., Durham, P. J. and Temmerman, W. M., Proc. Int. Conf. on High-Temperature Superconductors, Interlaken (1988) (to be published).
14. Macfarlane, R. M., Rosen, H. and Seki, H., Solid State Commun. **63**, 831 (1987).
15. Yamanaka, A., Minami, F., Wanatabe, K., Inoue, K., Takekawa, S. and Iyl, N., Jpn. J. Appl. Phys. **26**, 1404 (1987).
16. Cardona, M., Genzel, L., Liu, R., Wittlin, A., Mattausch, H. J., Garcia-Alvarado, F. and Garcia-Gonzalez, E., Solid State Commun. **64**, 727 (1987).
17. Morioka, Y., Kikuchi, M. and Syono, Y., Jpn. J. Appl. Phys. **26**, 1499 (1987).
18. Bonn, D. A., Greedan, J. E., Stager, C. V., Timusk, T., Doss, M. G., Herr, S. L., Kamarás, K. and Tanner, D. B. Phys. Rev. Lett. **58**, 2249 (1987).
19. Thomsen, C., Liu, R., Bauer, M., Wittlin, A., Genzel, L., Cardona, M., Schönherr, E., Bauhofer, W. and König, W., Solid State Commun. **65**, 55 (1988).
20. Saito, Y., Sawada, H., Iwazumi, T., Abe, Y., Ikeda, H. and Yoshizaki, R., Solid State Comun. **64**, 1047 (1987).
21. Knoll, P. and Kiefer, W., Proc. Int. Discussion Meeting on High Temperature Superconductors, Mauterndorf (1988) (to be published).
22. Iwazumi, T., Naki, I., Izumi, M., Dyanagi, H., Sawada, H., Ikeda, H., Saito, Y., Abe, Y., Takita, K. and Yoshizaki, R., Solid State Commun. **65**, 213 (1988).
23. Stavola, M., Cava, R. J. and Rietman, E. A., Phys. Rev. Lett. **58**, 1571 (1987).
24. Weber, W., Private communication.
25. Blumenröder, S., Zirngiebl, E., Schmidt, H., Güntherodt, G. and Brenten, H., Solid State Commun. **64**, 1229 (1987).
26. Thomsen, C., Cardona, M., Kress, W., Liu, R., Genzel, L., Bauer, M., Schönherr, E. and Schroder, U., Solid State Commun. (to be published).
27. Liu, R., Thomsen, C., Kress, W., Cardona, M., Gegenheimer, B., de Wette, F. W., Prade, J., Kulkarni, A. D. and Schroder, U., To be published.